Dynamic metabolic and molecular changes during seasonal shrinking in *Sorex araneus*

William R. Thomas, Cecilia Baldoni, Yuanyuan Zeng, et al.

Genome Res. 2026 36: 61-70 originally published online November 4, 2025
Access the most recent version at doi:10.1101/gr.280639.125

Dynamic metabolic and molecular changes during seasonal shrinking in *Sorex araneus*

William R. Thomas,[1] Cecilia Baldoni,[2,3] Yuanyuan Zeng,[4] David Carlson,[1] Julie Holm-Jacobsen,[4] Marion Muturi,[2] Dominik von Elverfeldt,[5] Tue B. Bennike,[4] Dina K.N. Dechmann,[2,3] John Nieland,[4] Angelique P. Corthals,[6,9] and Liliana M. Dávalos[1,7,8,9]

[1]*Department of Ecology and Evolution, Stony Brook University, Stony Brook, New York 11794, USA;* [2]*Max-Planck Institute of Animal Behavior, Radolfzell 78315, Germany;* [3]*University of Konstanz, Konstanz 78464, Germany;* [4]*Health Science and Technology, Aalborg University, Gistrup 9260, Denmark;* [5]*Division of Medical Physics, Department of Diagnostic and Interventional Radiology, University Medical Center Freiburg, Faculty of Medicine, University of Freiburg, Freiburg 79106, Germany;* [6]*John Jay College of Criminal Justice, New York, New York 10019, USA;* [7]*Institute for Advanced Computational Science, Stony Brook University, Stony Brook, New York 11794, USA;* [8]*Consortium for Inter-Disciplinary Environmental Research, Stony Brook University, Stony Brook, New York 11794, USA*

To meet the challenge of wintering in place, many high-latitude small mammals reduce energy demands through hibernation. In contrast, short-lived Eurasian common shrews, *Sorex araneus*, remain active and shrink, including energy-intensive organs in winter, regrowing in spring in an evolved strategy called Dehnel's phenomenon. How this size change is linked to metabolic and regulatory changes to sustain their high metabolism is unknown. Here, we analyze metabolic, proteomic, and gene expression profiles spanning the entirety of Dehnel's seasonal cycle in wild shrews. We show regulatory changes to oxidative phosphorylation and increased fatty acid metabolism during autumn-to-winter shrinkage, as previously found in hibernating species. But in shrews, we also find upregulated winter expression of genes involved in gluconeogenesis: the biosynthesis of glucose from noncarbohydrate substrates. Coexpression models reveal changes in size and metabolic gene expression coordinated via FOXO signaling, whose overexpression reduces size and extends life span in many model organisms. We propose that although shifts in gluconeogenesis meet the challenge posed by high metabolic rate and active winter lifestyle, FOXO signaling is central to Dehnel's phenomenon, with spring downregulation limiting life span in these shrews.

[Supplemental material is available for this article.]

Wintering adaptations vary widely across animals, and the most common strategies are conserving energy by lowering metabolic rates and activity (e.g., hibernation or torpor) and migration. In contrast, a handful of species that neither migrate nor slow their metabolism have evolved a different wintering size plasticity known as Dehnel's phenomenon (Dehnel 1949; Pucek 1965b; Lázaro et al. 2018; Lázaro and Dechmann 2021). This pattern of growth, best studied in the Eurasian common shrew, *Sorex araneus*, is unlike that of almost every other mammal. Instead of growing continuously to adulthood, juvenile *S. araneus* grow to an initial maximum size in the first summer of their disproportionately brief life (~1 year). In anticipation of harsh winter conditions, shrews then shrink, reaching a nadir in winter, followed by rapid regrowth to their adult, breeding size in spring. This plasticity is not just a retooling of overall body size but also occurs in many vital organs, including the liver, brain, and spleen (Pucek 1965a,b). Although Dehnel's phenomenon has garnered much interest because of its potential for regenerating organs (Ray et al. 2020), metabolic and regulatory changes during this wintering adaptation remain largely unknown.

Dehnel's phenomenon corresponds to the unique physiological constraints shrews face. *S. araneus* have one of the highest mammalian metabolic rates measured to date (Genoud et al. 2018), requiring high and constant food intake throughout the year (Keicher et al. 2017). But supplying energy to maintain this high metabolic rate is especially difficult in the autumn and winter, when temperatures decrease and resources become scarce (Hyvärinen 1984; Churchfield et al. 2012). Therefore, Dehnel's phenomenon is construed as an evolutionary adaptation that compensates for continuously high energetic demands by reducing body and organ size, particularly of energy-expensive tissue (Lázaro et al. 2019). In support of this hypothesis, the absolute resting metabolic rate decreases with shrew size in winter, whereas the mass-specific rate remains the same (Hyvärinen 1984; Taylor et al. 2013; Schaeffer et al. 2020).

Wintering strategies encompass a spectrum of related traits and physiological processes (Auteri 2022). Changes in other wintering strategies, such as metabolic shifts observed in hibernation (Boyer and Barnes 1999; Chazarin et al. 2019; Weir et al. 2024),

[9]**These authors contributed equally to this work.**
Corresponding authors: william.thomas@stonybrook.edu, liliana.davalos@stonybrook.edu

Article published online before print. Article, supplemental material, and publication date are at https://www.genome.org/cgi/doi/10.1101/gr.280639.125. Freely available online through the *Genome Research* Open Access option.

may thus share common mechanisms with those involved in Dehnel's phenomenon. For example, mechanistic analyses of mammalian hibernation have identified a toolkit of genes that regulates vast metabolic changes (Boyer and Barnes 1999; Faherty et al. 2016; Chazarin et al. 2019), including those associated with increased fatty acid oxidation (Villanueva-Cañas et al. 2014), as hibernators rely on gradual fat utilization over winter. Research on shrew physiology indicates they also rely extensively on lipid metabolism in winter (Keicher et al. 2017) and may share some molecular mechanisms with hibernation.

But *S. araneus* remains active throughout winter, undergoing drastic shrinkage while navigating a metabolically demanding environment. This active wintering strategy contrasts with hibernation, suggesting key differences in metabolic and regulatory processes. For example, wintering shrews show rapid fat turnover, with 50% fat turnover rates decreasing from 4.5 h in summer juveniles to 2.5 h in winter (Keicher et al. 2017). Consequently, metabolic profiles may differ significantly between these strategies. In hibernators, there is also a downregulation of genes involved in glucose breakdown (Villanueva-Cañas et al. 2014). In general, when energy stores are depleted, glucose is produced in the liver through gluconeogenesis. This glucose is then released into the bloodstream and metabolized in the mitochondria via oxidative phosphorylation (Rui 2014). Unlike hibernators that suppress this response, wintering shrews seem to increase this starvation response as environments become harsher (Hyvärinen 1984). Thus, we hypothesized that shrews shrink by upregulating fatty acid metabolism, with potential similarities to hibernators, although, unlike hibernators, shrews supplement their energy budget with glucose to maintain their active winter lifestyle.

To examine metabolic dynamics and regulatory changes throughout Dehnel's phenomenon, and its potential parallels to other wintering strategies, we conducted a multiomic analysis of *S. araneus* across seasonal time points that match the trajectory of size plasticity. We focused on blood, which circulates metabolites, and the liver, a key site of metabolic regulation including lipid and glucose processing. By integrating phenotypic, metabolomic, transcriptomic, and proteomic data, our study aims to identify the molecular pathways that orchestrate seasonal changes in body size and to explore how these pathways may be linked to metabolism and longevity in small, actively wintering mammals.

Results

Dehnel's phenomenon in a German shrew population

Comparisons of body mass throughout the cycle confirmed patterns of size changes (Fig. 1A). Analyzing the 24 shrews collected for all stages of Dehnel's phenomenon (large summer juvenile = 5; shrinking autumn juvenile $n = 4$; small winter juvenile $n = 5$; regrowing spring adult $n = 5$; regrown summer adult $n = 5$) (Supplemental Data S1; Supplemental Table S1), we found (*t*-test) body mass shrank as expected between summer juveniles and winter juveniles (body mass = −1.00 g, $P = 0.03$) with regrowth as they matured to spring adults (body mass = +3.72 g, $P < 0.0001$) (Supplemental Table S2). Shrew liver mass reached a minimum as autumn juveniles (liver mass = −0.09 g, $P = 0.09$) (Supplemental Table S3), with the significant portion of regrowth occurring between the winter juvenile and spring adult phases (liver mass = +0.54 g, $P < 0.001$). These size changes both validated previous research and were used to guide metabolomic, transcriptomic, and proteomics characterization of Dehnel's phenomenon.

Metabolomic shifts in lipid metabolite concentrations

We characterized the blood plasma metabolome (Supplemental Data S2) to quantify metabolites throughout the cycle and evaluated the potential shifts in metabolism during shrinkage and

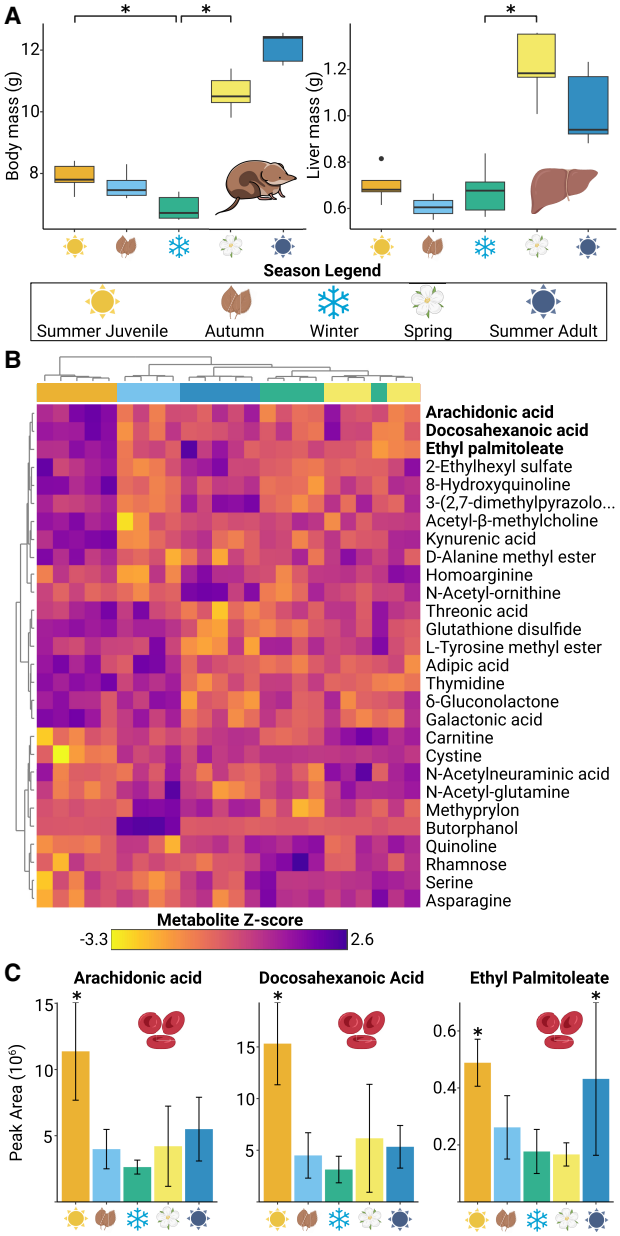

Figure 1. Confirming Dehnel's phenomenon and metabolic profiling of the blood metabolome. (*A*) Mass change of body and liver through a year of Dehnel's phenomenon. Both the body and the liver begin to decrease in mass as autumn juveniles, with body mass at a minimum as winter juveniles, proceeded by regrowth as spring adults. Asterisks represent significant size changes (adjusted $P < 0.05$). (*B*) Heatmap of 28 statistically significant differentially concentrated metabolites between stages of Dehnel's phenomenon. Hierarchical clustering using these significant metabolite groups each profile into each season. (*C*) Three of these metabolites were lipid metabolites (ethyl palmitoleate, docosahexanoic acid, arachidonic acid), with decreases in autumn, winter, and spring individuals.

regrowth. We validated 250 metabolites found in all seasons with multiple detection methods (Supplemental Data S3). Normalized concentrations of these metabolites clustered according to season (Supplemental Fig. S1A,B). We found 28 with significant differences in mean concentration across the stages of Dehnel's phenomenon ($P < 0.05$) (Fig. 1B; Supplemental Table S4; Supplemental Fig. S1C). Among the differentially concentrated metabolites, three were lipid metabolites: arachidonic acid (AA; $P = 0.04$, $F = 5.78$), ethyl palmitoleate (EP; $P = 0.02$, $F = 6.79$), and docosahexanoic acid (DHA; $P = 0.04$, $F = 5.86$). These three lipid metabolites showed significant decreases in peak area, a proxy for concentration, between summer juveniles and other stages of size change (autumn juveniles, winter juveniles, spring adults), especially in winter juveniles (AA = -8.7×10^7 peak area, DHA = -1.2×10^8 peak area, EP = -3.1×10^6 peak area), for which the concentrations of DHA and AA were at their minimum.

Global liver gene expression patterns reflect seasonal body size plasticity

To understand how gene expression in the liver changes across seasonal stages, and whether these shifts align with the body size changes of Dehnel's phenomenon, we began by examining the global transcriptomic patterns (Supplemental Data S4). Exploratory analyses of liver gene expression revealed patterns that mirror seasonal changes in body size. Using a likelihood ratio test (LRT), we compared the full model (~sex+season) to a null model with only an intercept (~1). This test identified 3336 genes whose expression was significantly associated with seasonal stage ($P_{adj} < 0.01$) (Supplemental Data S4). Principal component analysis (PCA) of these significant genes showed clear seasonal clustering, with PC1 and PC2 explaining 22.3% and 13.4% of the variation, respectively (Supplemental Fig. S2A). Hierarchical clustering supports this structure, grouping samples into three major clusters: one composed of summer juveniles, another including shrinking autumn and winter juveniles, and a third encompassing spring and summer adults (Supplemental Fig. S2B).

To investigate the temporal dynamics of gene regulation, we further clustered the 3336 significant genes based on their expression patterns across seasons (Fig. 2B; Supplemental Fig. S2C). This analysis distinguished four gene expression clusters with more than 150 genes (Supplemental Data S4). Clusters 1 ($n = 580$ genes) and 2 ($n = 156$ genes) displayed consistent increases or decrease in expression across time points, suggesting that they are more reflective of ontogeny than of seasonal plasticity. In contrast, clusters 3 ($n = 312$ genes) and 4 ($n = 887$ genes) exhibited expression changes consistent with Dehnel's phenomenon. Specifically, cluster 3 genes were downregulated during shrinkage (autumn and winter) and strongly upregulated during regrowth. Conversely, cluster 4 genes showed the opposite pattern: upregulated during shrinkage and downregulated as body size increased. Between clusters 3 and 4, only two pathways were significantly enriched: protein processing in the endoplasmic reticulum ($P_{adj} < 0.0001$) and proteosome ($P_{adj} < 0.05$) (Supplemental Data S4; Supplemental Table S5).

Transcriptomic signatures of winter shrinkage

Results showed many differentially expressed genes in the liver between summer juveniles and winter juveniles (shrinking stage), with an upregulation of genes related to mitochondrial, lipid, and glucose metabolism (Supplemental Data S5). Comparisons revealed 964 differentially expressed genes ($P_{adj} < 0.05$), with 497 significantly upregulated and 467 significantly downregulated in winter juveniles (Fig. 3A). We then used a ranked gene set enrichment test to identify functional effects of RNA regulatory change. This analysis identified 25 pathways enriched with differentially expressed genes (21 upregulated and four downregulated) (Fig. 4A; Supplemental Data S5). Oxidative phosphorylation was the most enriched pathway ($P_{adj} < 0.001$, normalized enrichment score = 2.34, [NES]), consisting of 46 genes. This gene set included 21 upregulated genes that encode mitochondrial complex I subunit proteins (NDUFs) and 19 upregulated genes encoding ATPases and synthases (Supplemental Fig. S3), suggesting pathway activation. Other important pathways, based on initial hypotheses from previous Dehnel's research described in the Introduction, enriched with upregulated genes included glycolysis and gluconeogenesis ($P_{adj} < 0.001$, NES = 2.09) (Supplemental Fig. S4), which contained the gene encoding for glucose 6-phosphatase catalytic subunit 1 (*G6PC1*; $P_{adj} = 0.41$, log fold change [LFC] = 0.30) (Fig. 4B), and fatty acid metabolism ($P_{adj} < 0.01$, NES = 1.81) (Supplemental Fig. S5).

Proteomic validation of metabolic pathway shifts

We validated changes in metabolism-related gene expression between summer juveniles and winter juveniles (shrinking stage) with liver proteomics (Supplemental Data S6). Despite the liver proteomics ($n = 1377$ proteins) data set being smaller than the gene expression set ($n = 24{,}205$ transcripts), there was substantial overlap in direction, significance, and pathway enrichment of changes between the two (Supplemental Fig. S6; Supplemental Fig. S3). Using a linear model to estimate the correlation between differential change (summer juveniles vs. winter juveniles) in gene expression and protein abundance, we found that LFC in gene expression was significantly associated with LFC in protein abundance ($F = 197.5$, $df = 1373$, $P < 0.001$), but the model only explains a fraction of the variation between them ($R^2 = 0.13$) (Fig. 3A). However, this correlation is congruent with overall correlation between protein abundance and RNA expression across all seasons for gene in both data sets ($R^2 = 0.14$) (Supplemental Fig. S6). Analyzing differential abundance of proteins, we found 124 proteins significantly changed ($P_{adj} < 0.05$) between summer juveniles and winter juveniles (78 increased and 46 decreased in winter) (Fig. 3A). Thirty-four of these proteins overlapped with differentially expressed genes, all but one with matching mRNA and protein direction.

Ranked set enrichment for proteomics identified five enriched pathways ($P_{adj} < 0.05$), four of which overlapped the RNA pathway enrichment (oxidative phosphorylation, Parkinson's disease, Alzheimer's disease, Huntington's disease). Oxidative phosphorylation was the most enriched pathway in both mRNA and protein expression and included 17 overlapping genes/proteins, 11 of which were found to be significant in at least one of the data sets (*ATP5MG*, *NDUFB4*, *PPA1*, *SDHB*, NDUFV3, NDUFA6, NDUFB8, NDUFS3, ATP5PO, NDUFC2, NDUFS6; all in the same direction). Proteomic analysis did not reveal upregulation in the glycolysis/gluconeogenesis ($P_{adj} = 1.00$, NES = 0.66) pathway, although all but one overlapping gene also increased in abundance in proteomics, including three aldehyde dehydrogenase genes (*ALDH3A2*, $P_{adj} < 0.01$, LFC = 0.64; *ALDH1B1*, $P_{adj} < 0.01$, LFC = 0.81; *ALDH9A1*, $P_{adj} = 0.47$, LFC = 0.35) (Fig. 4B). Similarly, proteomic set enrichment analysis did not validate fatty acid metabolism enrichment ($P_{adj} = 0.91$, NES = 1.00), but there was overlap (11 of

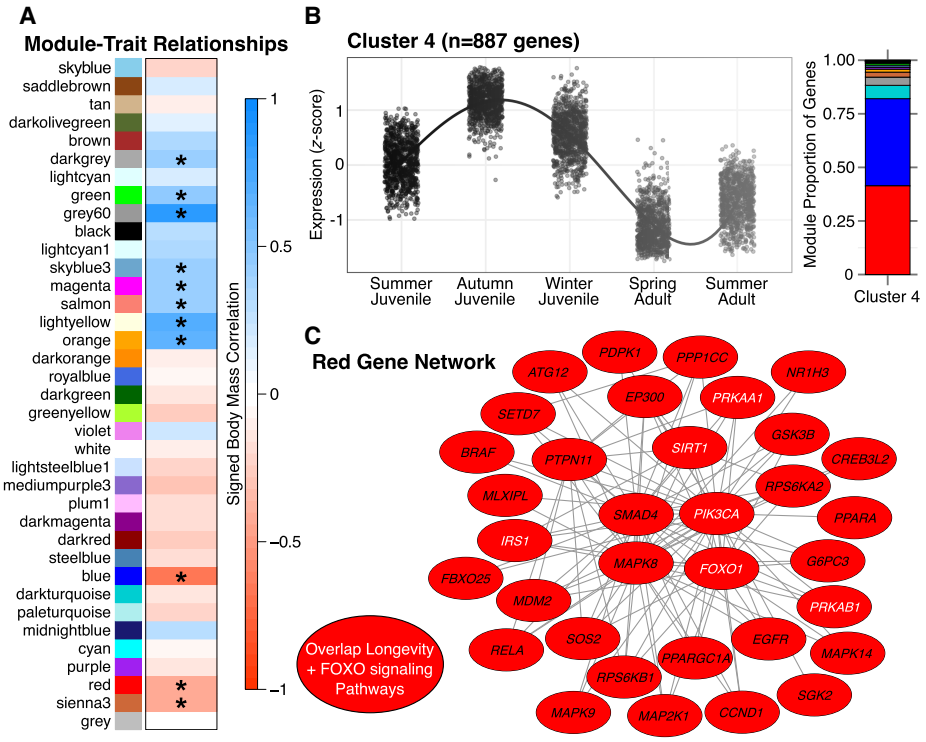

Figure 2. Gene networks highly correlated with seasonal body size plasticity. (*A*) Gene expression correlations form 37 modules. Eleven of these modules were significantly correlated with shrew body size. (*B*) Clustering of significant genes across seasons (LRT, $P_{adj} < 0.05$) revealed a cluster of genes (cluster 4) with upregulation during shrinking seasons. The largest proportion of these genes overlapped with the red gene network. (*C*) Pathway enrichment of the large ($n = 3268$ genes) "red" module highlighted functional associations to FOXO signaling and insulin resistance (plotted genes), which are associated with longevity regulating pathways.

18 genes), including genes that encode proteins that transport (*ACADM*, $P_{adj} = 0.17$, LFC = 0.40; *ACADVL*, $P_{adj} = 0.26$, LFC = 0.35) and breakdown of long fatty acid chains (*ACOX1*, $P_{adj} < 0.001$, LFC = 0.81).

Comparison to hibernation reveals distinct gene expression signatures

To assess whether Dehnel's phenomenon shares regulatory features with hibernation, we compared differentially expressed genes in winter shrew livers to those identified in hibernating *Mesocricetus auratus* (Syrian hamsters). Overlap between the two data sets was limited (Supplemental Table S6): Only nine genes were significantly upregulated in both species, whereas 22 were significantly downregulated in both (FDR/$P_{adj} < 0.05$) (Supplemental Fig. S7). An additional 19 genes overlapped but in opposite directions. Two overlapping genes (*ALDH1B1* and *GPI*) are components of the glycolysis and gluconeogenesis pathway, as well as *ETNPPL*, a fasting-induced gene.

Pathway enrichment corroborates gene expression discordance between the two wintering strategies. Only four pathways were significantly enriched in hibernating *M. auratus* (Supplemental Data S7), and none overlapped with those enriched in wintering shrews. Those included proximal tubule bicarbonate reclamation ($P_{adj} < 0.05$, NES = 2.01), circadian rhythm ($P_{adj} < 0.05$, NES = 1.92), MAPK signaling ($P_{adj} < 0.05$, NES = 1.71), and terpenoid backbone biosynthesis ($P_{adj} < 0.01$, NES = −2.14). Although oxidative phosphorylation showed some signal of upregulation in *M. auratus* (NES = 1.58), it was not statistically significant ($P_{adj} = 0.15$).

Spring regrowth exhibits weaker transcriptomic and proteomic signals

Comparisons between winter juveniles and spring adults (growth) showed extensive change in gene expression coincident with metabolic change, but correlation with proteomics was weak (Fig. 3B). Of 2462 significantly differentially expressed genes, 1130 were upregulated and the rest downregulated in spring adults (Fig. 3B), yet differential mRNA expression only significantly enriched two pathways, including the downregulation of the cell cycle ($P_{adj} < 0.05$, NES = −1.77) and proteosome ($P_{adj} < 0.05$, NES = −1.91) pathways (Supplemental Data S8). Comparing protein abundance between winter juveniles and spring adults (growth), 183 proteins showed significant change (42 increased and 141 decreased) (Fig. 3B; Supplemental Data S9). Although 41 of these overlapped with significant differentially expressed genes, nearly a quarter of them (10) were in the opposite direction. This is unsurprising, as the model between protein LFC and mRNA LFC explains little variation ($R^2 = 0.02$, F = 22.73, df = 1374, $P < 0.001$) (Fig. 3B). Ranked protein enrichment corroborated minimal correlation, as none of the six significant pathways—starch and sucrose metabolism ($P_{adj} < 0.01$, NES = 2.33); TCA cycle ($P_{adj} < 0.01$, NES = 2.28); cysteine and methionine metabolism ($P_{adj} < 0.05$, NES = 2.13); valine, leucine, and isoleucine degradation ($P_{adj} < 0.05$, NES = 1.92); spliceosome ($P_{adj} < 0.05$, NES = −1.71); and cell adhesion molecules ($P_{adj} < 0.05$, NES = −1.75)—overlapped with mRNA gene set analyses. There were, however, individual genes validated in a change of direction with proteomic data found in upregulated processes in winter juveniles that decreased in spring adults (LFC < 0): oxidative phosphorylation (*NDUFB4*, *PPA1*),

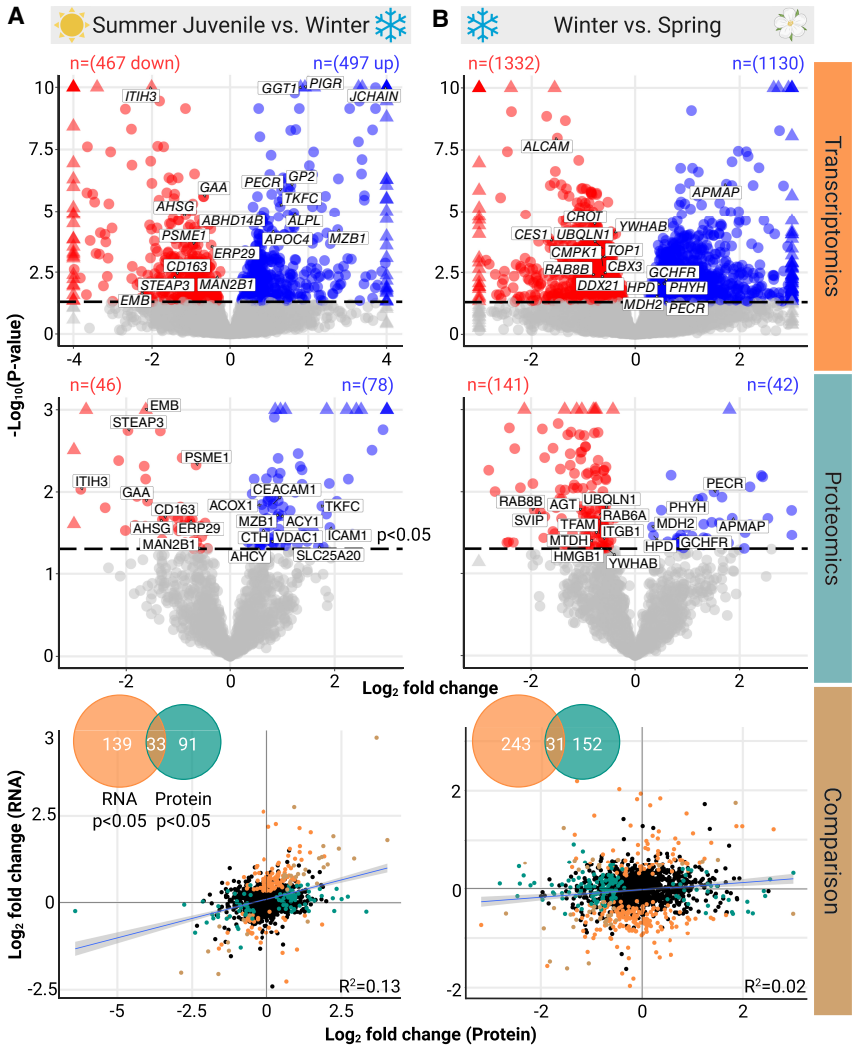

Figure 3. Seasonal regulatory (transcriptomics and proteomics) changes in the shrew liver. (*A*) Volcano plots of significant ($P_{adj}<0.05$) differentially expressed genes and proteins (colored) for summer versus winter juvenile comparisons. Triangles represent lower *P*-values (−log(*P*) > 10) or log fold changes (abs (LFC) > 4) beyond the limits of the graph. Correlation of log fold change and significant gene overlap between RNA and protein indicates high association between multiomic comparisons ($R^2 = 0.13$). (*B*) Although volcano plots of significant differentially expressed genes and proteins for winter juveniles versus spring adult were identified, multiomic correlation was low in comparison to the shrinking phase ($R^2 = 0.02$).

gluconeogenesis (*ALDH3A2*, *PGK1*, *ALDH1B1*), and fatty acid metabolism (*ACOX1*).

Network analysis identifies FOXO signaling pathways regulating size plasticity

Differential expression analyses focused on genes of high effect between two size extremes, but large modules comprising genes of *small* effect could also play pivotal roles in regulating metabolic changes across all seasons. We characterized interactions in expression among genes and identified modules of coexpressed liver genes correlated with body size using a weighted gene coexpression network analysis (WGCNA) (Supplemental Data S10). We identified 37 modules (Fig. 2A), 11 of which were significantly associated with body size ($P<0.05$). Among these, the "grey60" module is a small gene network most positively correlated with larger body size ($n=352$ genes, $P<0.001$, r = 0.85, df = 21) and the "blue" module is a large network positively correlated with small body size ($n=3224$ gene, $P<0.001$, r = −0.65, df = 21). However, the "red" module was significant ($n=3224$ gene, $P<0.05$, r = −0.41, df = 21) and had the highest proportion (0.414) of genes that overlapped with cluster 4 genes, which were upregulated during autumn and winter. Although no KEGG pathways were significant after multiple test correction when testing for gene set enrichment from the "grey60" module, metabolic pathways were highly significant ($P<0.01$). The "blue" module enriched 10 KEGG pathways, including the proteasome ($P_{adj}<0.01$, nucleocytoplasmic transport ($P_{adj}<0.01$, and autophagy in animals ($P_{adj}<0.01$). Thirty-four KEGG pathways from the "red" module significant genes were significant after multiple test correction ($P_{adj}<0.05$). These pathways included FOXO signaling ($P_{adj}<0.01$), as well as pathways upstream (MAPK signaling, $P_{adj}<0.05$) and downstream (insulin resistance, $P_{adj}<0.01$; longevity regulating pathways, $P_{adj}<0.05$) of this pathway (Fig. 2C; Supplemental Table S7).

Discussion

Eurasian common shrews, *S. araneus*, require constant food intake to sustain their extraordinarily high metabolic rates throughout the year (Genoud et al. 2018). Maintaining their energetic budget is particularly difficult in winter, as temperatures drop, along with available food. Within a German shrew population, we found clear signs of a seasonal size plasticity known as Dehnel's phenomenon (Fig. 1A; Dehnel 1949; Pucek 1965b; Lázaro et al. 2018). These shrews shrink in autumn through winter, with recovery in the ensuing spring. Using this population with confirmed Dehnel's phenomenon, we identify seasonal changes to metabolism and underlying regulatory processes.

We hypothesized that shrews rely on fat utilization to maintain metabolic homeostasis in winter, as do hibernators, but unlike them, shrews rapidly turn over fat during shrinkage (Keicher et al. 2017). Both hibernators and winter shrews may experience similar depleted energy reserves, as suggested by the shared upregulation of *ETNPPL*, a gene typically induced by fasting in mice to regulate lipid homeostasis (White et al. 2021). Despite this common signal of energetic stress, transcriptomic analyses of winter juvenile shrews revealed upregulation of key lipid metabolism genes, including those involved in promoting fatty acid oxidation: acyl-CoA dehydrogenase medium chain (*ACADM*), acyl-CoA

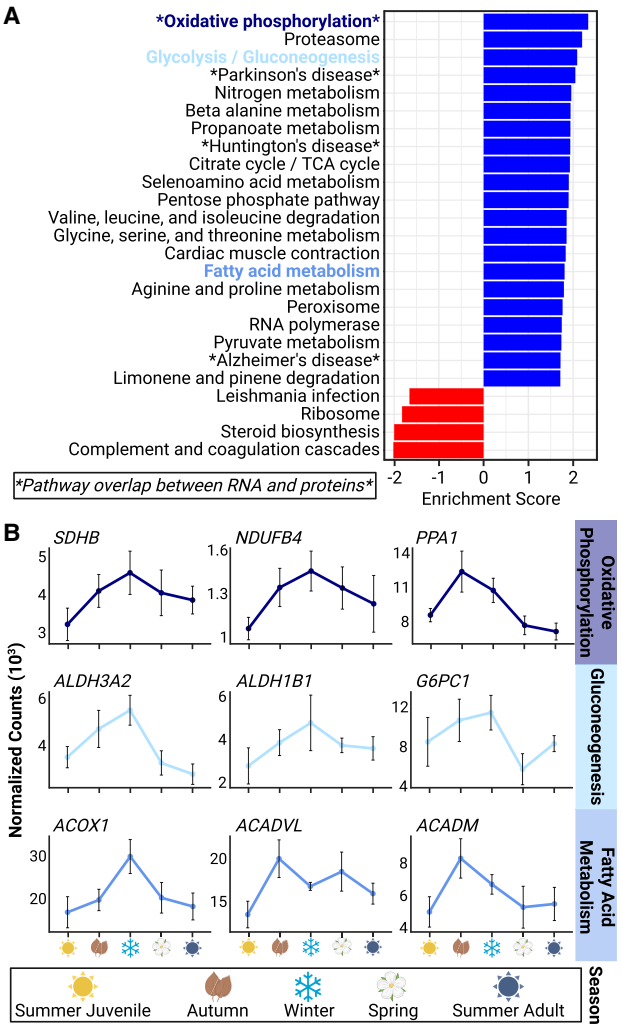

Figure 4. Seasonal changes in pathways associated with Dehnel's phenomenon. (*A*) Pathway enrichment of summer versus winter juveniles between RNA (shown) and protein analyses, both with the largest enrichment of oxidative phosphorylation pathways. (*B*) Normalized gene counts in seasonally changing pathways of interest.

dehydrogenase very long chain (*ACADVL*), and acyl-CoA oxidase 1 (*ACOX1*) (Fig. 4B). Analysis of gene and protein expression within this pathway (Supplemental Fig. S5) supports activation of fatty acid oxidation (Fig. 4A), but we cannot fully rule out potential inhibitory effects without functional validations. For example, *ACOX1* encodes the rate-limiting enzyme for oxidizing very long chain fatty acids and is critical for interorgan metabolic communication. Liver-specific knockouts of *Acox1* in mice increase adipose tissue browning and circulating levels of polyunsaturated omega-3 fatty acids (Lu et al. 2024).

Consistent with the role of *ACOX1* in lipid metabolism, in shrunken winter juvenile shrews we observe an increase in *ACOX1* expression paired with a decrease in circulating levels of polyunsaturated fatty acids (DHA and AA) (Fig. 1B,C). This contrasts with hibernators: Circulating DHA and AA rise significantly in wintering bears and hibernating arctic ground squirrels (Drew et al. 2001; Elaine Epperson et al. 2011; Chazarin et al. 2019; Rice et al. 2021). Regulatory similarities and metabolomic differences indicate hibernation and Dehnel's wintering strategies rely upon lipid metabolism in the liver. Although hibernators conserve fat reserves over winter, shrews exhibit rapid fat turnover (Keicher et al. 2017), decreasing levels of polyunsaturated fatty acids as they maintain activity in winter.

Regulatory changes related to mitochondrial function further highlight differences in metabolic processes between Dehnel's phenomenon and hibernation. The strongest signal in both RNA and protein expression was the upregulation of oxidative phosphorylation pathways in winter juveniles, indicating pathway activation (Fig. 4A). These include 21 genes encoding mitochondrial complex I subunit proteins (NDUFs) and the succinate dehydrogenase gene, *SDHB*. Hibernators monitor energy expenditure through circadian rhythm pathways (Supplemental Fig. S3) and conserve energy in part through reduced liver mitochondrial oxidation in response to cold temperature (Chaffee et al. 1961; Staples and Brown 2008), decreasing SDH activity (Gehnrich and Aprille 1988; Armstrong and Staples 2010). This, in turn, impairs cellular respiration as they lower body temperature and metabolic rate. In contrast, winter juvenile shrews show upregulated oxidative phosphorylation pathways compared with summer juveniles. Although Dehnel's phenomenon reduces resting metabolic rate in winter (Taylor et al. 2013), shrews remain active and neither reduce their body temperature nor upregulate circadian rhythm pathways as hibernators do. Mitochondrial regulation in shrews is therefore opposite to that of hibernators and may use known temperature-sensitive oxidative phosphorylation pathways to improve mitochondrial efficiency, enhance metabolic plasticity, or maintain internal temperatures despite the reduction in metabolic rate and body size. This hypothesis can be tested by examining mitochondrial oxygen consumption in the liver throughout Dehnel's phenomenon.

During autumn and winter, shrews appeared to meet their energetic needs by activating responses similar to those triggered by starvation. When blood sugar is low, mammals promote gluconeogenesis, a process in which the liver produces free glucose from noncarbohydrate substrates to avoid cellular starvation (Rui 2014). This process has previously been linked to seasonal size change in shrews (Hyvärinen 1984). Glucose 6-phosphatase (G6P) enzyme levels peak during autumn and decline through spring, suggesting gluconeogenesis is highest in autumn and early winter when snow is too scarce to offer insulation, increasing demand for glucose to prevent starvation. We discovered an upregulation of the gluconeogenesis pathways in winter juveniles (Fig. 4), including the overexpression of aldehyde dehydrogenases (*ALDH1B1* and *ALDH3A2*) and *G6PC1*. *G6PC1* encodes one of three subunits of G6PC, a key gluconeogenesis enzyme in the final step of gluconeogenesis, which catalyzes the formation of D-glucose that can then be released into the blood. We propose that upregulation of this gene, along with others in the pathway, modulates the previously observed increase in gluconeogenesis (Hyvärinen 1984). Alongside elevated lipid metabolism and oxidative phosphorylation, these findings indicate shrews maximize all available energy resources during winter (Fig. 4).

Large changes in mRNA and proteins only weakly supported one another when comparing winter juveniles to spring adults (Fig. 3B), but changes in gene networks across all seasons parallel regrowth (Fig. 2B). We identified a large network negatively correlated with body size and enriched with genes involved in FOXO and insulin signaling. Central to this network is the forkhead box transcription factor 1 (*FOXO1*), upregulated during shrinkage and downregulated during growth. In mice, FOXO1 stimulates

gluconeogenesis that promotes hepatic glucose production and release (Zhang et al. 2006; Matsumoto et al. 2007; Xiong et al. 2013), which can subsequently impede processes including lipid metabolism in response to fasting glucose levels (Zhang et al. 2006; Tikhanovich et al. 2013; Xiong et al. 2013; Yang et al. 2021). In shrinking and regrowing shrews, FOXO signaling may thus regulate organismal energy homeostasis and size by simultaneously regulating both glucose and lipid use to meet changing energy demands.

Increased FOXO signaling, however, may incur costs to shrew longevity. In model organisms such as *Caenorhabditis elegans*, *Drosophila*, mice, and humans, FOXO1 overexpression can reduce size and extend life span, whereas inhibition leads to aging and senescence (Hwangbo et al. 2004; Katic and Kahn 2005; Gami and Wolkow 2006; Satoh et al. 2013). Compared to other mammals, *S. araneus* evolved Dehnel's phenomenon, a rare size plasticity (Dehnel 1949; Pucek 1965b; Lázaro et al. 2018), as well as a disproportionately high metabolic rate (Taylor 1998) and short life span (Healy et al. 2014). FOXO1 cycling could explain this unique combination of traits. Should findings from model organisms apply in the shrew, FOXO1-dependent glucose utilization regulates shrinking, reducing mortality during harsh winters, but undermines shrew longevity when reversed in spring as a terminal investment for growth and reproduction. Genes within this network are therefore key candidates for exploring both the regulatory mechanisms of size change in Dehnel's phenomenon and links between metabolic change and life span in mammals.

Our study has limitations that should temper interpretation of individual genes and proposed functions. Both small sample sizes within seasons and the small effect size of spring regrowth reduce statistical power and limit the resolution of gene-level inference in wild species (Todd et al. 2016). Although exploring pathway-level analyses can mitigate these constraints, animal- or cell-based functional validations will be essential to test our hypotheses. For example, CRISPR knockouts could clarify the roles of genes like *SDHB* and *FOXO1* in regulating mitochondrial efficiency or blood glucose levels across seasons (Fig. 5). As several proposed mechanisms likely involve interorgan signaling, future studies should examine other tissues including adipose tissue, which mediates lipid turnover, and the brain, which undergoes extraordinary plasticity in Dehnel's phenomenon.

Our work provides a framework to examine how seasonal metabolic remodeling distinct from hibernation regulates body size and life span. We propose that shrews undergoing Dehnel's phenomenon regulate gene expression to deplete fat stores, increase gluconeogenesis, and alter oxidative phosphorylation in ways that seem coordinated by FOXO signaling (Fig. 5). These pathways are well-known regulators of aging and energy balance in model organisms and may represent a conserved regulatory axis linking metabolism, size, and life span across mammals. By uncovering molecular covariates of this rare wintering strategy, our findings open new directions for studying natural models of regeneration and their links to metabolic plasticity and longevity.

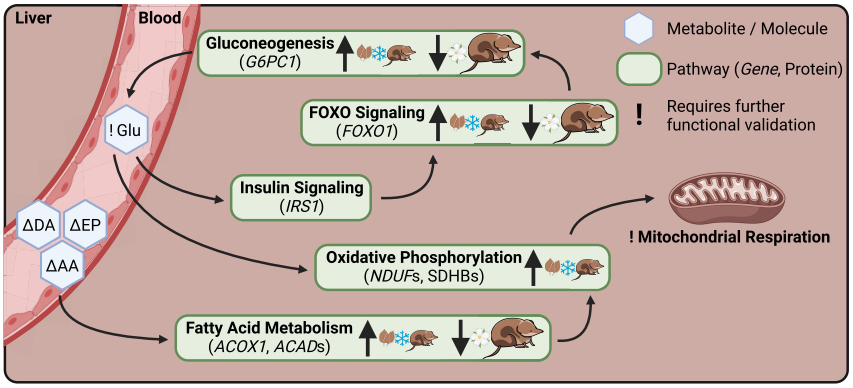

Figure 5. Summary of dynamic changes in shrew metabolism associated with seasonal size change, with proposed regulation of Dehnel's cycle. Depleted lipid metabolites in the blood and increased RNA expression of genes involved in fatty acid metabolism indicate rapid fat turnover in winter juveniles. FOXO signaling regulates gluconeogenesis, also upregulated in winter juveniles, providing another energy source. Both FOXO signaling and fatty acid metabolism promote changes in oxidative phosphorylation, as was found in both the transcriptomic and proteomic analyses, and have large effects on mitochondrial respiration in the liver.

Methods

Sample collection

Eurasian common shrews were trapped (protocols authorized by Regierungspräsidium Freiburg, Baden-Württemberg 35-9185.81/G-19/131) using insulated wooden traps in Radolfzell, Germany (47.9684 N, 8.9761 E), at five different stages of development: large summer juveniles ($n = 5$), shrinking autumn juveniles ($n = 4$), small winter juveniles ($n = 5$), regrowing spring adults ($n = 5$), and regrown summer adults ($n = 5$). Shrews were aged and sexed based on tooth wear, fur appearance, and gonad development prior to euthanasia. Fewer females than males were sampled in the juvenile stages ($n = 6$ females). At that age, shrews are prepubescent, not sexually dimorphic, and a previous study (Lázaro et al. 2018) found only minor sex dimorphism in brain region size change. Although female under sampling is unlikely to influence gene expression, sex was used as a covariate in subsequent models, accounting for this sampling skew.

Blood was collected prior to perfusion through the heart, stood for 15 min, and spun down at 1200 rpm; the serum pipetted off and then stored at −80°C. Shrews were perfused under anesthesia via the vascular system with PAXgene tissue fixative. Livers were removed and weighed to confirm the occurrence of Dehnel's phenomenon, split in half for paired transcriptomic and proteomic analyses, and then placed immediately into PAXgene tissue stabilizer. All samples were placed in stabilizer (2–24 h after extraction) and then stored in liquid nitrogen. Body and liver weights were tested for significant change in mass using a *t*-test between seasons.

Metabolomics

Metabolite analysis was carried out by MS-Omics using a Thermo Fisher Scientific vanquish LC (UPLC) coupled to Thermo Q exactive HF MS. Identification of compounds were performed at four levels: level 1—identification by retention times (compared against in-house authentic standards), accurate mass (with an accepted deviation of 3 ppm), and MS/MS spectra; level 2a—identification by retention times (compared against in-house authentic

standards), accurate mass (with an accepted deviation of 3 ppm); level 2b—identification by accurate mass (with an accepted deviation of 3 ppm); and MS/MS spectra. MetaboAnalyst was used to test for changes in concentration between seasons (Pang et al. 2021). Concentrations for each sample were normalized by the average concentration of summer adult samples, log-transformed, and auto-scaled (Supplemental Fig. S1A). A partial least-squares discriminant analysis was used to explore if classification of metabolites into clusters aligned with seasonality (Supplemental Fig. S1B). A one-way ANOVA was used to test for any significant seasonal difference in metabolite concentration, with *P*-values corrected with a false-discovery rate of 0.05 (Supplemental Fig. S1C). Within each significant metabolite, *t*-tests were used to identify pairwise differences in mean between each season. Samples were hierarchically clustered using significant genes and visualized using a heatmap (Fig. 1).

RNA sequencing

RNA was extracted with a modified Qiagen micro RNeasy protocol for small amounts of mammalian tissue (Yohe et al. 2020). RNA was sent to Genewiz for quality control, library preparation, and sequencing. RNA quantity was measured with a NanoDrop spectrophotometer, and quality of the RNA was assessed with RNA ScreenTape. Libraries were prepared with standard poly(A) selection and sequenced as 150 bp pair-end reads (Illumina, target of 15–25 million reads per sample).

Differential gene expression analysis

Tests for differential gene expression were conducted to identify genes whose liver expression changes during Dehnel's phenomenon. We trimmed adapters and filtered reads using fastp (Chen et al. 2018) and removed samples with extreme read counts (about 10-fold). Gene counts were quantified by pseudoaligning to the 24,205 protein coding genes of the *S. araneus* genome (mSorAra2; GCF_027595985.1) using kallisto (Bray et al. 2016). Counts were normalized for each tissue using DESeq2 median of ratios (Love et al. 2014) in R (R Core Team 2022).

Exploratory analyses included a PCA to assess global gene expression patterns across seasons. To identify genes associated with seasonal stage, we applied a LRT in DESeq2 (Love et al. 2014), comparing a full model that included sex and seasonal stage (~sex+season) to a reduced model with only an intercept (~1). Genes with an adjusted *P*-value < 0.01 were considered significantly associated with seasonal stage. Expression profiles of these significant genes were then clustered to explore temporal dynamics using DEGreport (v1.44) (https://bioconductor.org/packages/DEGreport). As these genes had already been filtered for statistical significance and lacked a continuous ranking metric such as −log fold change, we performed an unranked Gene Ontology (GO) enrichment of KEGG pathways using the DAVID gene functional classification tool (Huang et al. 2009). We chose KEGG over other GO sets, as KEGG's orthology mapping is easier to use for a nonmodel species such as *S. araneus*.

Next, summer juveniles and winter juveniles were compared to infer regulatory processes associated with shrinkage, whereas winter juveniles were tested against spring adults to explore processes linked to regrowth. Normalized counts for each gene were modeled as a function of sex and season with a negative binomial generalized linear model in DESeq2, and then, we used a Wald test to examine the statistical association between the log fold change and the season parameter, with *P*-values corrected using the Benjamini–Hochberg procedure (Benjamini and Hochberg 1995). We then identified significantly enriched pathways with differentially expressed genes using a ranked gene set enrichment of KEGG pathways using FGSEA (Korotkevich et al. 2021). We chose a ranked gene set enrichment as it avoids an arbitrary threshold of significance, considering the entire gene list of both upregulated and downregulated genes.

To compare gene expression during Dehnel's phenomenon to patterns observed in hibernation, we obtained liver transcriptomic results from hibernating *M. auratus* (Syrian hamsters, NCBI Gene Expression Omnibus [GEO; https://www.ncbi.nlm.nih.gov/geo/] accession number GSE199814) (Coussement et al. 2023). As small mammals with high metabolic rates, Syrian hamsters provide a physiologically comparable model to common shrews compared with large-bodied hibernators such as bears. We performed a ranked gene set enrichment analysis using the approach described above. To identify overlap, we compared significantly enriched pathways as well as individual genes ($P_{adj} < 0.05$) that were differentially expressed in both data sets.

Weighted gene coexpression network analysis

We used the WGCNA package (Langfelder and Horvath 2008) to create coexpression networks for the liver and determined if these correlations between genes were significantly correlated with body size. We calculated the Pearson's correlation for expression between each gene pair, which was then transformed to an adjacency matrix using a soft-threshold power adjacency function described by Langfelder and Horvath (2008). The power function reduced the spurious connectivity between genes from noise by increasing sensitivity, and its appropriate scale was determined by maximizing the scale-free topology criterion (maximizing model fit while saturating mean connectivity). The resulting adjacency matrix was then used to calculate a topological overlap matrix (dissimilarity matrix), in which dissimilarity distances grouped genes into modules using fuzzy, cmeans hierarchical clustering. We removed any module with fewer than 25 genes and merged gene modules that were found to have similar eigengene values. Then, eigengene significance between the correlation of body size to each module's eigengene value was calculated. Cytoscape (Shannon et al. 2003) was used to visualize significant networks and calculate network statistics such as node (gene) connectivity. Enrichments for each module were analyzed using DAVID to test for GO enrichment (Huang et al. 2009), and module genes were compared to those identified using the LRT.

Proteomics

Liver tissue from *S. araneus* was isolated, and protein homogenates were prepared by transferring the liver tissue to a dissection buffer containing 10% sucrose (VWR), imidazole (Merck Millipore), EDTA (Sigma-Aldrich), Pefabloc (Sigma-Aldrich), and leupeptin (VWR). The mixture was homogenized (T10 basic ULTRA-TURAX homogenizer IKA) for 20 sec; then, samples were centrifuged at 1000*g* for 15 min. Supernatants were stored at −20°C. Proteomic sample preparation was performed using a iST 96x kit (PreOmics 00027). The samples were vacuum-centrifuged overnight, and the dry peptide product was stored at −80°C until analysis.

Peptides were resuspended in a solution containing 2% acetonitrile (ACN), 0.1% formic acid (FA), and 0.1% TFA, and then, peptides were briefly sonicated. Five micrograms of total peptide material was analyzed per liquid chromatography–mass spectrometry analysis. Samples were analyzed using a UPLC-nanoESI MS/MS setup with a NanoRSLC system (Dionex). The system was coupled online with an emitter for nanospray ionization (New Objective PicoTip 360-20-10) to a Q exactive HF mass spectrometer (Thermo Fisher Scientific). The peptide material was loaded onto a 2 cm trapping reversed-phase Acclaim PepMap RSLC C18 column (Dionex) and separated using an analytical 75 cm reversed-phase

Acclaim PepMap RSLC C18 column (Dionex). Both columns were kept at 60°C. The sample was eluted with a gradient of 90% solvent A (0.1% FA, 0.1% TFA) and 10% solvent B (0.1% FA, 0.1% TFA in ACN), which was increased to 7% solvent B on a 1 min ramp gradient at a constant flow rate of 300 nL/min. Subsequently, the gradient was raised to 30% solvent B on a 45 min ramp gradient. The mass spectrometer was operated in positive mode, selecting up to 20 precursor ions with a mass window of m/z 1.6 based on highest intensity for higher-energy collisional dissociation (HCD) fragmenting at a normalized collision energy of 27. Selected precursors were dynamically excluded for fragmentation for 30 sec.

A label-free relative quantitation analysis was performed using MaxQuant 1.5.7.4 software (Tyanova et al. 2016a). Raw files were searched against the *S. araneus* genome assembly (GCF_027595985.1_mSorAra2.pri_genomic.gtf). All standard settings were employed with carbamidomethylation (C) as a static peptide modification and deamidation (NQ), oxidation (M), formylation (N-terminal and K), and protein acetylation (N-terminal) as variable modifications. The output contained a list of proteins identified at a <1% false-discovery rate, and their abundances were further filtered and processed using the Perseus v1.5.6.0 platform (Tyanova et al. 2016b). All reverse hits that identified proteins were removed from further analysis, and the data were $\log_2$-transformed to approximate a normal distribution. Two or more unique peptides were required for protein quantitation. Additionally, a nonzero quantitation value in at least 70% of the samples in one of the groups was required from quantifiable proteins. The mass spectrometry proteomics data have been deposited to the ProteomeXchange Consortium (http://proteomecentral.proteomexchange.org) (see Data access).

After preprocessing, we inferred potential functional changes associated with differences in protein abundances and analyzed correlations with transcriptomic data. First, the label-free quantitation matrix was restricted to summer-juvenile and winter-juvenile samples. Differential protein abundance was evaluated in Perseus (v1.5.6.0) with its permutation-based two-sided Student's *t*-test (250 randomizations; no group preservation). We corrected for multiple testing via the Benjamini–Hochberg procedure with a false-discovery rate of 5%. A S_0 constant of 0.1 was added to stabilize variance in the SAM-like statistic. Significantly differentially abundant proteins ($P_{adj} < 0.05$) were displayed in a volcano plot. We then identified significantly enriched pathways of protein using a ranked gene set enrichment of KEGG pathways using FGSEA (Korotkevich et al. 2021).

To investigate the relationship between seasonal changes in protein abundance and RNA abundance, we also quantified Pearson's correlation coefficients between log-transformed protein abundance and normalized RNA expression across all samples. We also performed two linear regression analyses to observe protein and RNA concordance. First, log-transformed RNA counts were modeled as a function of the corresponding protein abundance using the lm function in R. Second, differential protein abundance was modeled as a function of the corresponding gene expression log fold change.

Data access

The raw RNA sequencing data generated in this study have been submitted to the NCBI BioProject database (https://www.ncbi.nlm.nih.gov/bioproject/) under accession number PRJNA941271. The mass spectrometry proteomics data generated in this study have been submitted to the ProteomeXchange Consortium via the PRIDE partner repository (Perez-Riverol et al. 2025) with the data set identifier PXD068559 (doi: 10.6019/PXD068559). The raw metabolomics data generated in this study have been submitted to Metabolomics Workbench (Sud et al. 2016) with a project identifier PR002691, study ID ST004264 (doi: 10.21228/M8T837). Processed data and results can be found in the Supplemental Materials and are publicly available on Dryad (https://doi.org/10.5061/dryad.pc866t1w3). Reproducible code to complete these analyses can be found in the Supplemental Code and on GitHub (https://github.com/wrthomas315/Dehnels_Seasonal_RNAseq2/tree/main/data).

Competing interest statement

The authors declare no competing interests.

Acknowledgments

We thank Joshua Rest, Krishna Veeramah, and Tanya Lama, who have provided helpful feedback on initial results and previous versions of the manuscript. We thank Michal Oklinski for help with initial dissections. We also thank National Institutes of Health funding (U2C-DK119886 and OT2-OD030544) to Metabolomics Workbench for raw data submission. W.R.T. and research were supported by the Human Frontier Science Program Award (RGP0013/2019) to D.K.N.D., L.M.D., and J.N. and by the Stony Brook University Presidential Innovation and Excellence Fund to L.M.D.

Author contributions: L.M.D., D.K.N.D., A.P.C., and J.N. conceived and funded the project. C.B., M.M., and D.K.N.D. collected, measured, and sampled shrews. W.R.T. designed and conducted genomic analyses. W.R.T., J.H.-J., J.N., and A.P.C. analyzed metabolite concentrations. T.B.B. performed the LC/MS/MS and correlated with shrew database. W.R.T. and Y.Z. analyzed proteomic results. W.R.T. visualized data and wrote initial draft. L.M.D., D.K.N.D., J.N., D.C., and A.P.C. contributed to review and editing of draft. All authors contributed to data interpretation.

References

Armstrong C, Staples JF. 2010. The role of succinate dehydrogenase and oxaloacetate in metabolic suppression during hibernation and arousal. *J Comp Physiol B Biochem Syst Environ Physiol* **180:** 775–783. doi:10.1007/s00360-010-0444-3

Auteri GG. 2022. A conceptual framework to integrate cold-survival strategies: torpor, resistance and seasonal migration. *Biol Lett* **18:** 20220050. doi:10.1098/rsbl.2022.0050

Benjamini Y, Hochberg Y. 1995. Controlling the false discovery rate: a practical and powerful approach to multiple testing. *J R Stat Soc Ser B Stat Methodol* **57:** 289–300. doi:10.1111/j.2517-6161.1995.tb02031.x

Boyer BB, Barnes BM. 1999. Molecular and metabolic aspects of mammalian hibernation. *Bioscience* **49:** 713–724. doi:10.2307/1313595

Bray NL, Pimentel H, Melsted P, Pachter L. 2016. Near-optimal probabilistic RNA-seq quantification. *Nat Biotechnol* **34:** 525–527. doi:10.1038/nbt.3519

Chaffee RR, Hoch FL, Lyman CP. 1961. Mitochondrial oxidative enzymes and phosphorylations in cold exposure and hibernation. *Am J Physiol* **201:** 29–32. doi:10.1152/ajplegacy.1961.201.1.29

Chazarin B, Storey KB, Ziemianin A, Chanon S, Plumel M, Chery I, Durand C, Evans AL, Arnemo JM, Zedrosser A, et al. 2019. Metabolic reprogramming involving glycolysis in the hibernating brown bear skeletal muscle. *Front Zool* **16:** 12. doi:10.1186/s12983-019-0312-2

Chen S, Zhou Y, Chen Y, Gu J. 2018. fastp: an ultra-fast all-in-one FASTQ preprocessor. *Bioinformatics* **34:** i884–i890. doi:10.1093/bioinformatics/bty560

Churchfield S, Rychlik L, Taylor JRE. 2012. Food resources and foraging habits of the common shrew, *Sorex araneus*: Does winter food shortage explain Dehnel's phenomenon? *Oikos* **121:** 1593–1602. doi:10.1111/j.1600-0706.2011.20462.x

Coussement L, Oosterhof MM, Guryev V, Reitsema VA, Bruintjes JJ, Goris M, Bouma HR, De Meyer T, Rots MG, Henning RH. 2023. Liver transcriptomic and methylomic analyses identify transcriptional mitogen-activated protein kinase regulation in facultative hibernation of Syrian hamster. *Proc R Soc B Biol Sci* **290:** 20230368. doi:10.1098/rspb.2023.0368

Dehnel A. 1949. Studies of the genus *Sorex* L. *Ann Univ M Curie-Sklod* **4:** 17–104.
Drew KL, Rice ME, Kuhn TB, Smith MA. 2001. Neuroprotective adaptations in hibernation: therapeutic implications for ischemia-reperfusion, traumatic brain injury and neurodegenerative diseases. *Free Radic Biol Med* **31:** 563–573. doi:10.1016/S0891-5849(01)00628-1
Elaine Epperson L, Karimpour-Fard A, Hunter LE, Martin SL. 2011. Metabolic cycles in a circannual hibernator. *Physiol Genomics* **43:** 799–807. doi:10.1152/physiolgenomics.00028.2011
Faherty SL, Villanueva-Cañas JL, Klopfer PH, Albà MM, Yoder AD. 2016. Gene expression profiling in the hibernating primate, *Cheirogaleus medius*. *Genome Biol Evol* **8:** 2413–2426. doi:10.1093/gbe/evw163
Gami MS, Wolkow CA. 2006. Studies of *Caenorhabditis elegans* DAF-2/insulin signaling reveal targets for pharmacological manipulation of lifespan. *Aging Cell* **5:** 31–37. doi:10.1111/j.1474-9726.2006.00188.x
Gehnrich SC, Aprille JR. 1988. Hepatic gluconeogenesis and mitochondrial function during hibernation. *Comp Biochem Physiol B* **91:** 11–16. doi:10.1016/0305-0491(88)90107-1
Genoud M, Isler K, Martin RD. 2018. Comparative analyses of basal rate of metabolism in mammals: data selection does matter. *Biol Rev* **93:** 404–438. doi:10.1111/brv.12350
Healy K, Guillerme T, Finlay S, Kane A, Kelly SBA, McClean D, Kelly DJ, Donohue I, Jackson AL, Cooper N. 2014. Ecology and mode-of-life explain lifespan variation in birds and mammals. *Proc R Soc B: Biol Sci* **281:** 20140298. doi:10.1098/rspb.2014.0298
Huang DW, Sherman BT, Lempicki RA. 2009. Systematic and integrative analysis of large gene lists using DAVID bioinformatics resources. *Nat Protoc* **4:** 44–57. doi:10.1038/nprot.2008.211
Hwangbo DS, Garsham B, Tu MP, Palmer M, Tatar M. 2004. *Drosophila* dFOXO controls lifespan and regulates insulin signalling in brain and fat body. *Nature* **429:** 562–566. doi:10.1038/nature02549
Hyvärinen H. 1984. Wintering strategies of voles and shrews in Finland. In *Wintering ecology of small mammals* (ed. Merritt JF), Spec. Pub. Carnegie Mus. Natural Hist. 10, pp. 139–148. Carnegie Museum of Natural History, Pittsburgh.
Katic M, Kahn CR. 2005. The role of insulin and IGF-1 signaling in longevity. *Cell Mol Life Sci* **62:** 320–343. doi:10.1007/s00018-004-4297-y
Keicher L, O'Mara MT, Voigt CC, Dechmann DKN. 2017. Stable carbon isotopes in breath reveal fast metabolic incorporation rates and seasonally variable but rapid fat turnover in the common shrew (*Sorex araneus*). *J Exp Biol* **220:** 2834–2841. doi:10.1242/jeb.159947
Korotkevich G, Sukhov V, Budin N, Atryomov MN, Sergushichev A. 2021. Fast gene set enrichment analysis. bioRxiv doi:10.1101/060012
Langfelder P, Horvath S. 2008. WGCNA: an R package for weighted correlation network analysis. *BMC Bioinformatics* **9:** 559. doi:10.1186/1471-2105-9-559
Lázaro J, Dechmann DKN. 2021. Dehnel's phenomenon. *Curr Biol* **31:** R463–R465. doi:10.1016/j.cub.2021.04.006
Lázaro J, Hertel M, Sherwood CC, Muturi M, Dechmann DKN. 2018. Profound seasonal changes in brain size and architecture in the common shrew. *Brain Struct Funct* **223:** 2823–2840. doi:10.1007/s00429-018-1666-5
Lázaro J, Hertel M, Muturi M, Dechmann DKN. 2019. Seasonal reversible size changes in the braincase and mass of common shrews are flexibly modified by environmental conditions. *Sci Rep* **9:** 2489. doi:10.1038/s41598-019-38884-1
Love MI, Huber W, Anders S. 2014. Moderated estimation of fold change and dispersion for RNA-seq data with DESeq2. *Genome Biol* **15:** 550. doi:10.1186/s13059-014-0550-8
Lu D, He A, Tan M, Mrad M, El Daibani A, Hu D, Liu X, Kleiboeker B, Che T, Hsu FF, et al. 2024. Liver ACOX1 regulates levels of circulating lipids that promote metabolic health through adipose remodeling. *Nat Commun* **15:** 4214. doi:10.1038/s41467-024-48471-2
Matsumoto M, Pocai A, Rossetti L, DePinho RA, Accili D. 2007. Impaired regulation of hepatic glucose production in mice lacking the Forkhead transcription factor Foxo1 in liver. *Cell Metab* **6:** 208–216. doi:10.1016/j.cmet.2007.08.006
Pang Z, Chong J, Zhou G, De Lima Morais DA, Chang L, Barrette M, Gauthier C, Jacques PÉ, Li S, Xia J. 2021. MetaboAnalyst 5.0: narrowing the gap between raw spectra and functional insights. *Nucleic Acids Res* **49:** 388–396. doi:10.1093/nar/gkab382
Perez-Riverol Y, Bandla C, Kundu DJ, Kamatchinathan S, Bai J, Hewapathirana S, John NS, Prakash A, Walzer M, Wang S, et al. 2025. The PRIDE database at 20 years: 2025 update. *Nucleic Acids Res* **53:** D543–D553. doi:10.1093/nar/gkae1011
Pucek M. 1965a. Water contents and seasonal changes of the brain-weight in shrews. *Acta Theriol (Warsz)* **10:** 353–367. doi:10.4098/AT.arch.65-30
Pucek Z. 1965b. Seasonal and age changes in the weight of internal organs of shrews. *Acta Theriol (Warsz)* **10:** 369–438. doi:10.4098/AT.arch.65-31
Ray S, Li M, Koch SP, Mueller S, Boehm-Sturm P, Wang H, Brecht M, Naumann RK. 2020. Seasonal plasticity in the adult somatosensory cortex. *Proc Natl Acad Sci U S A* **117:** 32136–32144. doi:10.1073/pnas.1922888117
R Core Team. 2022. *R: a language and environment for statistical computing*. R Foundation for Statistical Computing, Vienna. https://www.R-project.org/.
Rice SA, Mikes M, Bibus D, Berdyshev E, Reisz JA, Gehrke S, Bronova I, D'Alessandro A, Drew KL. 2021. Omega 3 fatty acids stimulate thermogenesis during torpor in the Arctic Ground Squirrel. *Sci Rep* **11:** 1340. doi:10.1038/s41598-020-78763-8
Rui L. 2014. Energy metabolism in the liver. *Compr Physiol* **4:** 177–197. doi:10.1002/cphy.c130024
Satoh A, Brace CS, Rensing N, Cliften P, Wozniak DF, Herzog ED, Yamada KA, Imai SI. 2013. Sirt1 extends life span and delays aging in mice through the regulation of Nk2 homeobox 1 in the DMH and LH. *Cell Metab* **18:** 416–430. doi:10.1016/j.cmet.2013.07.013
Schaeffer PJ, O'Mara MT, Breiholz J, Keicher L, Lázaro J, Muturi M, Dechmann DKN. 2020. Metabolic rate in common shrews is unaffected by temperature, leading to lower energetic costs through seasonal size reduction. *R Soc Open Sci* **7:** 191989. doi:10.1098/rsos.191989
Shannon P, Markiel A, Ozier O, Baliga NS, Wang JT, Ramage D, Amin N, Schwikowski B, Ideker T. 2003. Cytoscape: a software environment for integrated models. *Genome Res* **13:** 2498–2504. doi:10.1101/gr.1239303
Staples JF, Brown JCL. 2008. Mitochondrial metabolism in hibernation and daily torpor: a review. *J Comp Physiol B Biochem Syst Environ Physiol* **178:** 811–827. doi:10.1007/s00360-008-0282-8
Sud M, Fahy E, Cotter D, Azam K, Vadivelu I, Burant C, Edison A, Fiehn O, Higashi R, Nair KS, et al. 2016. Metabolomics Workbench: an international repository for metabolomics data and metadata, metabolite standards, protocols, tutorials and training, and analysis tools. *Nucleic Acids Res* **44:** D463–D470. doi:10.1093/nar/gkv1042
Taylor JRE. 1998. Evolution of energetic strategies in shrews. In *Evolution of shrews* (ed. Wójcik JM, Wolsan M), pp. 309–346. Mammal Research Institute, Polish Academy of Sciences, Białowieza, Poland.
Taylor JRE, Rychlik L, Churchfield S. 2013. Winter reduction in body mass in a very small, nonhibernating mammal: consequences for heat loss and metabolic rates. *Physiol Biochem Zool* **86:** 9–18. doi:10.1086/668484
Tikhanovich I, Cox J, Weinman SA. 2013. Forkhead box class O transcription factors in liver function and disease. *J Gastroenterol Hepatol* **28:** 125–131. doi:10.1111/jgh.12021
Todd EV, Black MA, Gemmell NJ. 2016. The power and promise of RNA-seq in ecology and evolution. *Mol Ecol* **25:** 1224–1241. doi:10.1111/mec.13526
Tyanova S, Temu T, Cox J. 2016a. The MaxQuant computational platform for mass spectrometry-based shotgun proteomics. *Nat Protoc* **11:** 2301–2319. doi:10.1038/nprot.2016.136
Tyanova S, Temu T, Sinitcyn P, Carlson A, Hein MY, Geiger T, Mann M, Cox J. 2016b. The Perseus computational platform for comprehensive analysis of (prote)omics data. *Nat Methods* **13:** 731–740. doi:10.1038/nmeth.3901
Villanueva-Cañas JL, Faherty SL, Yoder AD, Albà MM. 2014. Comparative genomics of mammalian hibernators using gene networks. *Integr Comp Biol* **54:** 452–462. doi:10.1093/icb/icu048
Weir K, Vega N, Busa VF, Sajdak B, Kallestad L, Merriman D, Palczewski K, Carroll J, Blackshaw S. 2024. Identification of shared gene expression programs activated in multiple modes of torpor across vertebrate clades. *Sci Rep* **14:** 24360. doi:10.1038/s41598-024-74324-5
White CJ, Ellis JM, Wolfgang MJ. 2021. The role of ethanolamine phosphate phospholyase in regulation of astrocyte lipid homeostasis. *J Biol Chem* **297:** 100830. doi:10.1016/j.jbc.2021.100830
Xiong X, Tao R, DePinho RA, Dong XC. 2013. Deletion of hepatic FoxO1/3/4 genes in mice significantly impacts on glucose metabolism through downregulation of gluconeogenesis and upregulation of glycolysis. *PLoS One* **8:** e74340. doi:10.1371/journal.pone.0074340
Yang Z, Roth K, Agarwal M, Liu W, Petriello MC. 2021. The transcription factors CREBH, PPARa, and FOXO1 as critical hepatic mediators of diet-induced metabolic dysregulation. *J Nutr Biochem* **95:** 108633. doi:10.1016/j.jnutbio.2021.108633
Yohe LR, Davies KTJ, Simmons NB, Sears KE, Dumont ER, Rossiter SJ, Dávalos LM. 2020. Evaluating the performance of targeted sequence capture, RNA-seq, and degenerate-primer PCR cloning for sequencing the largest mammalian multigene family. *Mol Ecol Resour* **20:** 140–153. doi:10.1111/1755-0998.13093
Zhang W, Patil S, Chauhan B, Guo S, Powell DR, Le J, Klotsas A, Matika R, Xiao X, Franks R, et al. 2006. FoxO1 regulates multiple metabolic pathways in the liver effects on gluconeogenic, glycolytic, and lipogenic gene expression. *J Biol Chem* **281:** 10105–10117. doi:10.1074/jbc.M600272200

Received March 10, 2025; accepted in revised form October 29, 2025.